Article

Measurement of Heat Flow Transmitted through a Stacked-Screen Regenerator of Thermoacoustic Engine

Shu Han Hsu * and Tetsushi Biwa

Department of Mechanical Systems and Design, Tohoku University, Sendai 980-8579, Japan; biwa@m.tohoku.ac.jp
* Correspondence: hsu@amsd.mech.tohoku.ac.jp; Tel.: +81-022-795-3875

Abstract: A stacked-screen regenerator is a key component in a thermoacoustic Stirling engine. Therefore, the choice of suitable mesh screens is important in the engine design. To verify the applicability of four empirical equations used in the field of thermoacoustic engines and Stirling engines, this report describes the measurements of heat flow rates transmitted through the stacked screen regenerator inserted in an experimental setup filled with pressurized Argon gas having mean pressure of 0.45 MPa. Results show that the empirical equations reproduce the measured heat flow rates to a mutually similar degree, although their derivation processes differ. Additionally, results suggest that two effective pore radii would be necessary to account for the viscous and thermal behaviors of the gas oscillating in the stacked-screen regenerators.

1. Introduction

A random stack of mesh screens is used as a regenerator of many Stirling engines, including thermoacoustic Stirling engines [1], because it achieves a high surface-area-to-volume ratio and good thermal contact with the working gas. Wide varieties of mesh numbers and wire diameters allow for flexible choices, but choosing an appropriate mesh screen is often difficult. This difficulty is attributable to tortuous flow channels inherent to the stacked-screen regenerator, which poses an obstacle from a theoretical perspective. Many experimental studies [2–7] have addressed this issue in oscillatory flow with frequencies below several tens of Hertz, aiming at gaining fundamental knowledge related to the mechanical Stirling engine. In the frequency range of thermoacoustic engines, however, experimental studies remain insufficient because they usually operate at several tens to hundreds of Hertz [1,8–13], even up to 23 kHz [14].

Our previous studies have measured the flow resistance and the acoustic power production in the regenerator [15,16] in oscillatory flow of pressurized Ar gas with a maximum frequency of 100 Hz. The results obtained with small amplitude oscillations show good agreement with predictions obtained using thermoacoustic theory [17–19] when the regenerator is assumed as a bundle of cylindrical tubes having effective radius $r_0 = \sqrt{d_h d_w}/2$ proposed by Ueda et al. [20], where d_h and d_w, respectively, denote the hydraulic diameter and the mesh wire diameter. Recently, Hasegawa et al. [21], based on results of experiments conducted at different frequencies and a fixed oscillatory velocity amplitude (=2 m/s) in air at atmospheric pressure, have also reported the applicability of r_0 for predicting the axial heat flow transported by the oscillatory gas in the regenerator. Further applicability of r_0 should be examined with different gases while varying the velocity amplitude.

Swift and Ward [22] proposed a set of equations of momentum, energy, and mass conservation for a stacked-screen regenerator by adopting the steady-flow data of Kays and London plots [23]. The equations are incorporated into the thermoacoustic calculation program—Design Environment for Low-amplitude Thermoacoustic Energy Conversion (DeltaEC) [24]. Although DeltaEC is now regarded as a standard design tool in the field of thermoacoustic engines, direct experimental verification is necessary to ascertain the heat transfer coefficient estimated from steady flow data.

This study was undertaken to test the empirical equations proposed for the axial heat transport experimentally using gas oscillations in the stacked-screen regenerator, when pressurized Ar gas is used as the working gas. Results show that the thermoacoustic theory provides a good starting point for elucidating heat transport in stacked screen regenerators, but further improvements are expected to be necessary for a more quantitative estimation.

2. Axial Heat Flow Estimated by Empirical Equations

In thermoacoustic theory [17–19], heat transport by gas oscillations along the *x*-axis with angular frequency ω is given by a result of hydrodynamic transport of entropy as

$$Q = \frac{1}{2}\rho_{\mathrm{m}}T_{\mathrm{m}}\int \mathrm{Re}[s\widetilde{V}]dA, \tag{1}$$

where s and V, respectively, represent the complex amplitude of entropy oscillations and axial velocity oscillations of the gas, and ρ_{m} and T_{m}, respectively, denote the temporal mean density and temperature. In addition, $\mathrm{Re}[\cdots]$ and $\widetilde{\cdots}$, respectively, show the real part and conjugate of a complex number. The surface integration is done over the cross-sectional area of the flow channel. The complex amplitude s in Equation (1) is expressed using complex amplitudes P and T of the gas pressure and temperature as

$$s = -\frac{\beta}{\rho_{\mathrm{m}}}P + \frac{c_{\mathrm{p}}}{T_{\mathrm{m}}}T, \tag{2}$$

where β signifies the coefficient of thermal expansion and c_{p} stands for the isobaric heat capacity per unit mass. For flow channels with a regular shape, T is obtained analytically. It can be expressed in a simpler form when the gas is assumed as an ideal gas. In such a case, the heat flow is given explicitly as

$$Q = -\frac{1}{2}A\mathrm{Re}\left[gP\widetilde{\langle V \rangle}\right] + \frac{1}{2}A\frac{\rho_{\mathrm{m}}c_{\mathrm{p}}}{\omega}\mathrm{Im}[g_{\mathrm{D}}]\frac{dT_{\mathrm{m}}}{dx}\left|\langle V \rangle\right|^2 \tag{3}$$

$$\text{with}\quad g = \frac{\chi_\alpha - \widetilde{\chi_\nu}}{(1+\sigma)(1-\widetilde{\chi_\nu})}\quad \text{and}\quad g_{\mathrm{D}} = \frac{\chi_\alpha + \sigma\widetilde{\chi_\nu}}{(1-\sigma^2)\left|1-\chi_\nu\right|^2},$$

where σ, ω, and A, respectively, denote the Prandtl number of the gas, angular frequency of the oscillation, and the cross-sectional area of the flow channel. In the equation, $\langle\cdots\rangle$ denote the cross-sectional average. Furthermore, $|\cdots|$ and $\mathrm{Im}[\cdots]$ signify taking the absolute value and imaginary part of a complex number; χ_j $(j = \nu, \alpha)$ is the thermoacoustic function associated with the thermal diffusivity α and kinematic viscosity ν of the working gas. For a cylinder with radius r_0, χ_j is given as

$$\chi_j = \frac{2J_1\left[(i-1)\frac{r_0}{\delta_j}\right]}{(i-1)\frac{r_0}{\delta_j}J_0\left[(i-1)\frac{r_0}{\delta_j}\right]}, \tag{4}$$

where J_1 and J_0, respectively, represent the first-order and zeroth-order Bessel functions of the first kind, i signifies the imaginary unit, and $\delta_j\left(=\sqrt{2j/\omega}\right)$ denotes the thermal or viscous penetration depth. We test the applicability of effective radius $r_0 = \sqrt{d_{\mathrm{h}}d_{\mathrm{w}}}/2$ by inserting it into the equation above. Moreover, we compare Q obtained by Equation (3) with the experimental heat flow that exists in the stacked-screen regenerator.

Swift and Ward [22] adopted the heat transfer coefficient of the steady flow and assumed the relation of $\langle T \rangle = \langle VT \rangle / \langle V \rangle$ to obtain the cross-sectional average $\langle T \rangle$ in the stacked-screen regenerator as

$$\langle T \rangle_{\mathrm{S}} = \frac{\beta T_{\mathrm{m}}}{\rho_{\mathrm{m}} c_{\mathrm{p}}} Y P - \frac{1}{i\omega} \frac{dT_{\mathrm{m}}}{dx} G \langle V \rangle, \tag{5}$$

with

$$Y = \frac{\varepsilon_{\mathrm{s}} + (g_c + e^{2i\theta_P} g_v) \varepsilon_{\mathrm{h}}}{1 + \varepsilon_{\mathrm{s}} + (g_c + e^{2i\theta_T} g_v) \varepsilon_{\mathrm{h}}}, G = \frac{\varepsilon_{\mathrm{s}} + (g_c - g_v) \varepsilon_{\mathrm{h}}}{1 + \varepsilon_{\mathrm{s}} + (g_c + e^{2i\theta_T} g_v) \varepsilon_{\mathrm{h}}},$$

$$\varepsilon_{\mathrm{s}} = \frac{\phi \rho_{\mathrm{m}} c_{\mathrm{p}}}{(1 - \phi) \rho_{\mathrm{s}} c_{\mathrm{s}}}, \varepsilon_{\mathrm{h}} = \frac{i}{2b\sigma^{1/3}} \left(\frac{d_{\mathrm{h}}}{\delta_\alpha} \right)^2,$$

$$b = 3.81 - 11.29\phi + 9.47\phi^2,$$

$$\theta_P = \mathrm{phase}\left[\langle V \rangle\right] - \mathrm{phase}\left[P\right], \theta_T = \mathrm{phase}\left[\langle V \rangle\right] - \mathrm{phase}\left[\langle T \rangle\right],$$

$$g_c = \frac{2}{\pi} \int_0^{\pi/2} \frac{dz}{1 + Re_{\mathrm{h}}^{3/5} \cos^{3/5}(z)}, g_v = -\frac{2}{\pi} \int_0^{\pi/2} \frac{\cos 2z \, dz}{1 + Re_{\mathrm{h}}^{3/5} \cos^{3/5}(z)}, \tag{6}$$

where ϕ represents the volume porosity, and where both the solid density ρ_{s} and heat capacity c_{s} are safely assumed as much larger than those of the gas; Re_{h} denotes the Reynolds number given as $Re_{\mathrm{h}} = |\langle V \rangle| d_{\mathrm{h}}/\nu$ ($|\langle V \rangle|$ represents the magnitude of the complex velocity $\langle V \rangle$). The heat flow in Equation (1) is then given for an ideal gas as

$$Q \cong \frac{1}{2} A \rho_{\mathrm{m}} T_{\mathrm{m}} \mathrm{Re} \left[\langle s \rangle \widetilde{\langle V \rangle} \right], \tag{7}$$

with

$$\langle s \rangle = -\frac{1}{\rho_{\mathrm{m}} T_{\mathrm{m}}} P + \frac{c_{\mathrm{p}}}{T_{\mathrm{m}}} \langle T \rangle_{\mathrm{S}}. \tag{8}$$

We also compare Q given by Equation (7) with the value obtained from experimentation.

In contrast to the Swift–Ward formulation, Tanaka et al. and Gedeon and Wood experimentally obtained the Nusselt number Nu for oscillatory flows in the frequency range of the mechanical Stirling engine. Tanaka et al. obtained the Nusselt number from measurements conducted with a maximum oscillation frequency of 10 Hz [3], which is expressed as

$$Nu_{\mathrm{T}} = 0.33 Re_{\mathrm{h}}^{0.67}. \tag{9}$$

Gedeon and Wood also proposed their Nu-Re_{h} correlation [4] with oscillation frequency up to 120 Hz. They incorporated it into a Stirling machine design software code—Sage [25], which is given as

$$Nu_{\mathrm{G}} = \left(1 + 0.99 \left(Re_{\mathrm{h}} \sigma \right)^{0.66} \right) \phi^{1.79}. \tag{10}$$

Applicability of these empirical equations should be tested, but incorporating them into the thermoacoustic theory presents a difficult problem for several reasons [22]. Therefore, as a tentative method, we determine $\langle T \rangle$ by inserting these empirical Nusselt numbers into the following equation:

$$\langle T \rangle_{Nu} = \left(\rho_{\mathrm{m}} c_{\mathrm{p}} + \frac{16}{i\omega} \frac{kNu}{d_{\mathrm{h}}^2} \right)^{-1} P - \left(i\omega + \frac{16}{\rho_{\mathrm{m}} c_{\mathrm{p}}} \frac{kNu}{d_{\mathrm{h}}^2} \right)^{-1} \frac{dT_{\mathrm{m}}}{dx} \langle V \rangle. \tag{11}$$

Equation (11) is obtained from Equation (27) of Reference [22] by introducing complex notation for $\langle T \rangle$ and by replacing the heat transfer coefficient h with $h = 4kNu/d_h$ while using thermal conductivity k of the gas. The heat flow can be estimated by inserting $\langle T \rangle_{Nu}$ into Equation (8) and by then using

Equation (7). Although this derivation would not qualify as a legitimate procedure, as we show later, it yields heat flows adequately to a similar degree to those of other methods tested in this study.

3. Experiments

Figure 1 presents the experimental setup, which consists of a stainless steel cylindrical tube with radius $R = 20$ mm and eight loudspeakers (FW168N; Fostex Co., Tokyo, Japan). The tube was filled with Ar gas of mean pressure of 0.45 MPa, which is one of the frequently used working fluids of the thermoacoustic engine. It contains a 35-mm-long regenerator and two 20-mm-long heat exchangers with temperatures T_H and T_R (=293 K). Regenerators of two kinds were employed: randomly stacked stainless-steel woven wire mesh screens (with mesh number of #20, #30, #50, #60, and #80) and a cylindrical ceramic honeycomb catalyst. Table 1 presents geometrical parameters of the wire meshes and ceramic honeycomb used for this study. The hydraulic diameter of the stacked-screen regenerator described in Table 1 was calculated as $d_h = \phi d_w / (1 - \phi)$. The cylindrical ceramic honeycomb catalyst possesses regular flow channels made of square pores of $d_h \times d_h$. Table 1 also includes parameters of the ceramic honeycomb catalyst.

Table 1. Geometrical properties of regenerators.

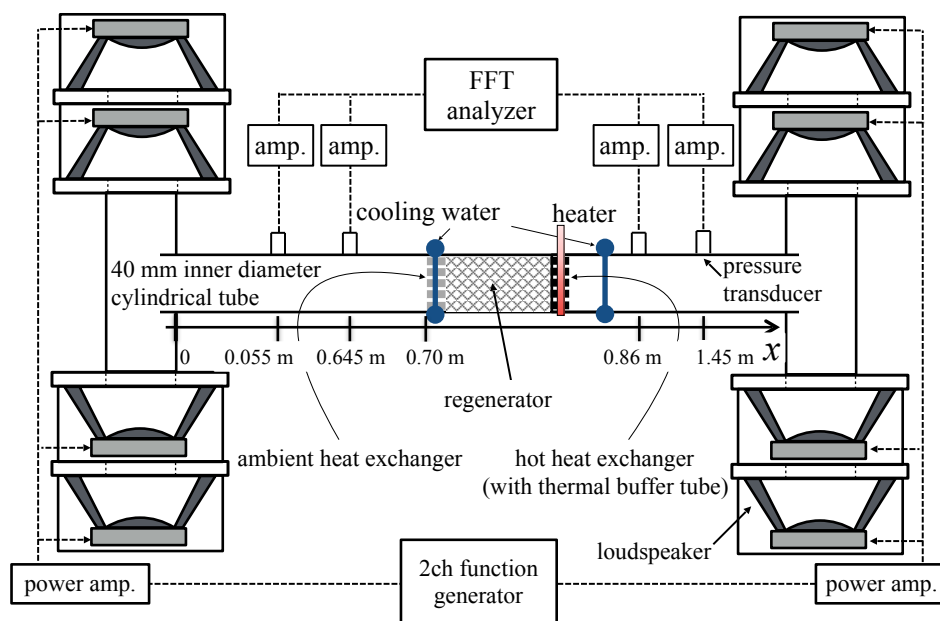| Stacked-Screen Regenerator			
Mesh Number	Wire Diameter (mm)	Hydraulic Diameter (mm)	Volume Porosity
#20	0.2	1.30	0.87
#30	0.22	0.80	0.78
#50	0.14	0.47	0.77
#60	0.12	0.40	0.77
#80	0.12	0.28	0.70
Ceramic Honeycomb Catalyst			
Cell Number		Hydraulic Diameter (mm)	Volume Porosity
1200		0.68	0.89

Figure 1. Schematic diagram of the experimental setup.

The hot heat exchanger with temperature T_H was heated using three electrical heater rods, whereas the ambient heat exchanger with T_R was cooled by running water around it. Temperatures T_H and T_R

were monitored using Type-K thermocouples placed on the central axis and at the regenerator ends, from which we determined the axial temperature difference $\Delta T = T_H - T_R$ across the regenerator. One end of a 50-mm-long thermal buffer tube region, next to the hot heat exchanger, was also cooled by running water.

The experimental procedure is explained as follows. First, in the absence of acoustic oscillations, a steady non-oscillating state with ΔT = 250 K was established. The necessary heating power was recorded as Q_{OFF}, which turned out to be 75 W with the change of ± 4 W at most, depending on the mesh number and ambient temperature. Second, we turned on the loudspeakers at ends of the tube to excite acoustic oscillations in the setup. In the presence of acoustic oscillations, the heat power Q_{ON}, which is necessary to maintain the steady oscillation state with ΔT = 250 K, was increased from Q_{OFF}, which means that the oscillatory flows cause additional heat transport along the regenerator. Therefore, we determined the rate of heat flow passing through the regenerator as

$$|Q| = Q_{ON} - Q_{OFF}. \tag{12}$$

Measurements were repeated four times for each experimental condition to obtain the mean value and the standard deviation of the measured $|Q|$. Because the heat flow Q is directed in the negative x-direction, we discuss the heat flow rate $|Q|$ for brevity.

During the measurements, gas oscillations were measured using two pairs of pressure transducers (PD104; JTEKT Corp., Osaka, Japan) mounted on the sidewall of the cylindrical tube at the positions presented in Figure 1. From the pressure amplitudes and phases obtained with a 24 bit fast Fourier transform analyzer (DS-3100; Ono Sokki Co. Ltd., Yokohama, Japan), we evaluated the acoustic pressure field $p(x) = \text{Re}\left[P(x)\exp\left(i\omega t\right)\right]$ and the velocity field $\langle u(x) \rangle = \text{Re}\left[\langle U(x) \rangle \exp\left(i\omega t\right)\right]$ in the 40-mm tube using the two-sensor method [26,27]. The complex amplitude $\langle V \rangle$ of the cross-sectional average velocity in the hot end of the regenerator was derived as $\langle V \rangle = \langle U_H \rangle / \phi$ from the continuity of volume velocity, where subscript H denotes the location at the hot end of the tube.

Throughout the experiments, the loudspeakers were controlled by voltage signals fed from a two-channel function generator via power amplifiers. By adjusting the phase difference and amplitude of the driving voltage signals, the specific acoustic impedance, given by the ratio $P_H / \langle U_H \rangle$ of complex amplitudes of pressure and velocity, was tuned to have magnitude of $0.3\rho_m a \pm 20\%$ and phase angle of $0° \pm 30°$ at the position of the hot end of the regenerator. It should be noted that the efficient thermoacoustic Stirling engines achieved the specific acoustic impedance as high as $30\rho_m a$ in the regenerator region [1]. In the present experimental setup, although it was equipped with eight loudspeakers, was not capable of producing such a high acoustic impedance while maintaining the magnitude of the velocity amplitude.

This amplitude ratio simplifies the first term Q_A on the right-hand side of Equation (3), and the ratio Q_A over the second term Q_D on the right-hand side of Equation (3) is then given as

$$\frac{Q_A}{Q_D} = \frac{\text{Re}\left[g\right]}{\text{Im}\left[g_D\right]} \frac{0.3a\omega}{c_p\left(dT_m/dx\right)}. \tag{13}$$

In the case of the regular flow channel regenerator made of the ceramic honeycomb catalyst, the amplitude ratio Q_A / Q_D was always below 0.09 for the present experimental conditions. For this reason, we can expect that the heat flow Q is well approximated by Q_D, and therefore a quadratic function of $|\langle V \rangle|^2$. For reference, we evaluated the ratio Q_A / Q_D for stacked screen regenerators by inserting Ueda's effective radius r_0 into Equation (3). Results showed that $Q_A / Q_D < 0.1$ for all mesh screens employed. Therefore, if the result of the thermoacoustic theory is also applicable to the stacked-screen regenerator, then Q would also be approximated as Q_D. We use this result to elucidate the function $\text{Im}\left[g_D\right]$ experimentally, after the comparison of Q determined using the empirical equations and using experimentation.

4. Results and Discussion

4.1. Regular Flow Channel Regenerator

Figure 2 presents relations between the heat flow rate $|Q|$ and the axial mean oscillation velocity amplitude $|\langle V \rangle|$ at the hot end of the regenerator region for the ceramic honeycomb catalyst. The experimental $|Q|$ values were obtained using oscillation frequencies of 5 Hz and 200 Hz. Results show that the experimental $|Q|$ increases quadratically with $|\langle V \rangle|$, as expected from Equation (3). For comparison, we evaluated heat flow rate $|Q|$ and $|Q_D|$ as a function of $|\langle V \rangle|$ by inserting the relation $P = 0.3\rho_m a\phi\,|\langle V \rangle|$, the experimental angular frequency ω and thermal properties of the gas at hot end temperature T_H into Equation (3). The temperature gradient, dT_m/dx, was approximated with the ratio of temperature difference ΔT over the regenerator length (=35 mm), and also half of the hydrodynamic diameter, $d_h/2 = 0.34$ mm, was used as the channel radius. The cross-sectional area A was determined as $A = \phi\pi R^2$, where R is the tube radius. Results show that $|Q|$ and $|Q_D|$ are mutually close, as described in the preceding section. Furthermore, good agreement is observed between the theoretical heat flows and the measured ones. These results confirm the validity of the thermoacoustic theory. It is noteworthy that the agreement between theoretical and experimental $|Q|$ is still good, even when $|\langle V \rangle| \approx 1$ m/s with 5 Hz. The corresponding displacement amplitude becomes as large as 31 mm, which is comparable to the regenerator length (=35 mm). This result indicates that the thermoacoustic theory that assumes a uniform channel is still useful for such a large amplitude regime.
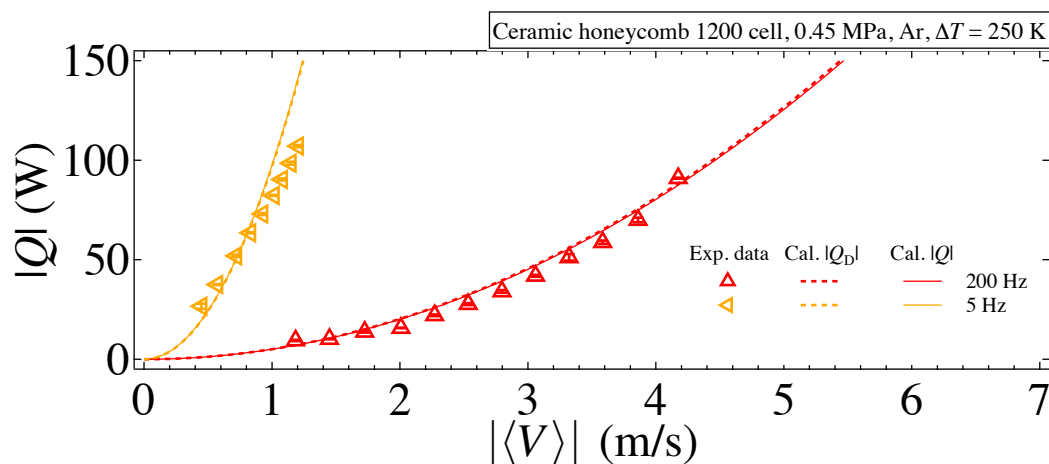

Figure 2. Comparison between the experimental heat flow rate $|Q|$ and theoretical calculations is given by Equation (3) for the ceramic honeycomb catalyst, where experimentally obtained results are shown as symbols with error bars. The theoretical calculations of $|Q|$ and $|Q_D|$ are shown, respectively, as solid and dashed curves.

4.2. Stacked-Screen Regenerator

Figure 3 presents the relation between the heat flow rate $|Q|$ and the velocity amplitude $|\langle V \rangle|$ for the mesh screens in Table 1, for 200 Hz frequency of the oscillatory flow. For comparison with the empirical equations, we show the measured $|Q|$ values in the four graphs Figure 3a–d. Solid symbols, each of which corresponds to meshes listed in Table 1, show that $|Q|$ increases quadratically with $|\langle V \rangle|$, as in the case of the regular flow channel regenerator.

Figure 3a compares the measured $|Q|$ with that obtained by inserting Ueda's effective radius r_0 into Equations (3) and (4), which shows good agreement with #50, #60, and #80 meshes, but slight deviation is visible for #20 and #30 meshes. Although the effective radius r_0 proposed by Ueda et al. was obtained from measurements at uniform temperature, the present experimentally obtained results

confirm the usefulness of evaluating the heat flow in the stacked-screen regenerator when Ar is the working gas.
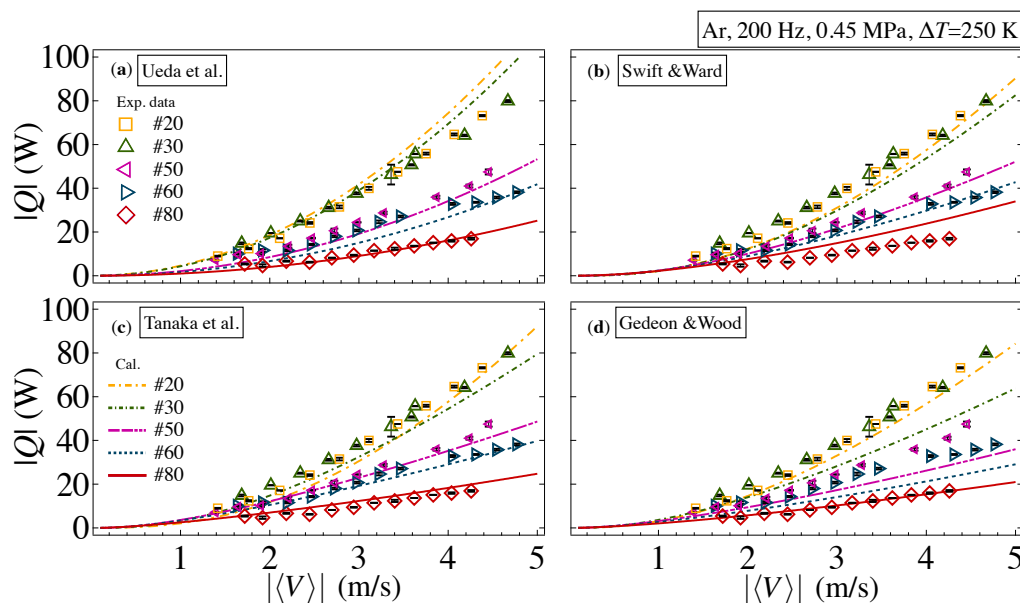

Figure 3. Experimental heat flow rate $|Q|$ and predictions given by respective empirical equations cited in this study for stacked-screen regenerators tested in pressurized helium gas with 0.45 MPa and with oscillation frequency of 200 Hz. Each panel presents identical experimentally obtained results by symbols with error bars. The empirical predictions are given, respectively, as (**a**) for Ueda et al.; (**b**) for Swift and Ward; (**c**) for Tanaka et al.; and (**d**) for Gedeon and Wood.

Comparison with results of the simple harmonic analysis derived by Swift and Ward is presented in Figure 3b, where curves are shown using Equations (5)–(8). For Equations (6), θ_T was estimated from Equation (4.68) of Reference [17] using $d_h/2$. Figure 3b shows that good agreement is obtained, except for the #80 mesh. Because the frequency of 200 Hz gives the thermal penetration depth $\delta_\alpha = \sqrt{2\alpha/\omega} = 0.15$ mm, these results indicate that the empirical expression of Swift and Ward is suitable for derivation of $|Q|$, when $d_h/(2\delta_\alpha)$ is in the range of $d_h/(2\delta_\alpha) > 1$, even though they assumed good thermal contact between the oscillation gas and the solid wall of the flow channel [24].

Heat flows estimated using the empirical equations of Tanaka et al. and Gedeon and Wood are shown, respectively, in Figure 3c,d, where we used Equations (9) and (10) to derive the temperature $\langle T \rangle_{Nu}$ in Equation (11). Then, we used Equations (7) and (8). All curves in Figure 3c show agreement with the measured $|Q|$ to a similar degree to those portrayed in Figure 3a,b. Actually, Figure 3d shows poor agreement with meshes of #30, #50, and #60, but the estimation is not bad overall. These results indicate that these empirical equations are applicable to thermoacoustic Stirling engines that operate at higher oscillation frequencies than the mechanical Stirling engines [3,4].

To assess the frequency dependence of the heat flow Q, the regenerator stacked with #30 mesh screens was tested with frequencies of 140 Hz and 180 Hz in the manner described above. Results are presented in Figure 4a–d, where the experimental $|Q|$ values increased slightly because of the decrease of the frequency. Figure 4a shows that the agreement with the effective radius of Ueda et al. was satisfactory. The Swift–Ward formulation in Figure 4b also works well, probably because of the value $d_h/(2\delta_\alpha)$ beyond 2 with those frequencies. The empirical equation of Tanaka et al. in Figure 4c agrees with the measured $|Q|$, although only the tendency of $|Q|$ for the frequency change is reproduced by the empirical equation of Gedeon and Wood, as shown in Figure 4d.
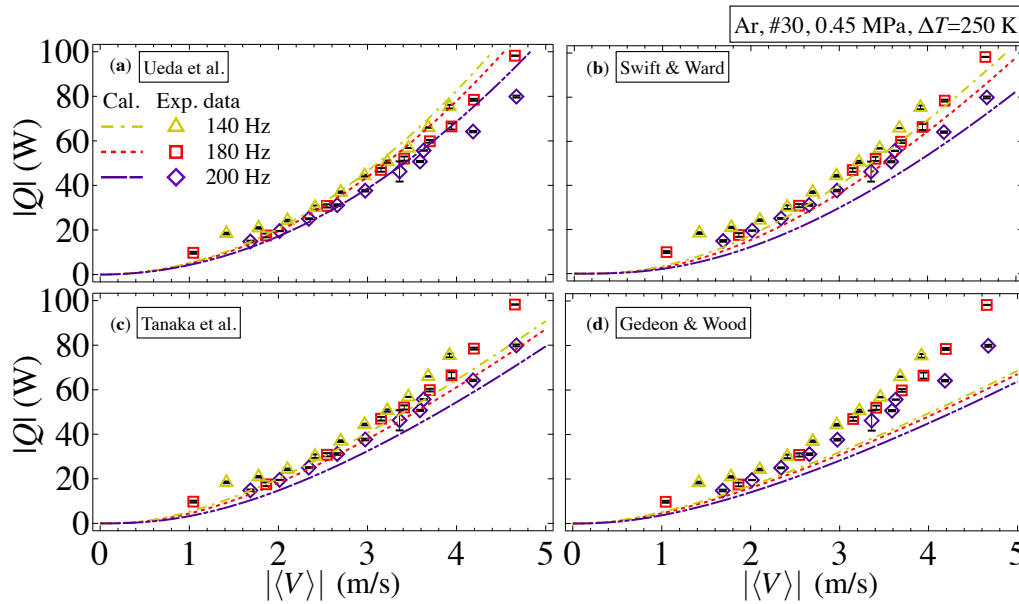
Figure 4. Comparisons between the experimental heat flow $|Q|$ and predictions given by the empirical equations. The mesh number of the stacked screens is #30. The working gas is Ar gas with 0.45 MPa. The test frequencies are 140, 180, and 200 Hz. Every panel presents the same experimentally obtained results by symbols with error bars, and empirical predictions are given respectively as the following: (**a**) for Ueda et al.; (**b**) for Swift and Ward; (**c**) for Tanaka et al.; and (**d**) for Gedeon and Wood.

4.3. Discussion

We have presented, through comparisons with experimentally obtained values, that the empirical equations proposed up to this point are useful as a first approximation to the heat flow in the stacked-screen regenerators, in spite of the considerable difference between their derivations. Among them, Ueda's formulation is the simplest to handle because of the absence of the Nusselt number Nu, which changes with the Reynolds number, Re_h, through the velocity amplitude $|V|$. Hereinafter, to strengthen the applicability of r_0 further, we investigate the function $\mathrm{Im}\,[g_\mathrm{D}]$ from the experimental $|Q|$.

As described in Section 3, the heat flow component Q_A is negligibly small compared to Q_D for all experimental conditions. Therefore, we approximate Q with Q_D, to express $\mathrm{Im}\,[g_\mathrm{D}]$ as

$$\mathrm{Im}\,[g_\mathrm{D}] = \frac{2}{A}\frac{\omega}{\rho_\mathrm{m}c_\mathrm{p}}\frac{Q}{(dT_\mathrm{m}/dx)\,|\langle V \rangle|^2}. \tag{14}$$

All factors in Equation (14) were evaluated using the measured values and the thermal properties of the gas at the hot end of the regenerator (T_H=543 K). The resulting $\mathrm{Im}\,[g_\mathrm{D}]$ is shown in Figure 5, after averaging over different values of $|\langle V \rangle|$. Additionally, the error bars attached on the symbols denote the standard deviations, which show the degree of the influence of $|\langle V \rangle|$. The curve represents $\mathrm{Im}\,[g_\mathrm{D}]$ given using $\sigma = 0.66$. It is apparent that $\mathrm{Im}\,[g_\mathrm{D}]$ obtained by Equation (14) roughly approximates the theoretical value for the cylindrical flow channel, which means that non-dimensional quantity r_0/δ_α captures the mechanism of the oscillation-induced heat flow in the stacked-screen regenerator. This finding is consistent with the results presented by Hasegawa et al. [21], who used air at atmospheric pressure as the working gas. Therefore, we consider that the local heat transfer between the screen meshes and the working fluid would be governed mostly by the non-dimensional parameter r_0/δ_α. Therefore, the axial heat flow through the stacked screen regenerator is fundamentally described by Equation (3).
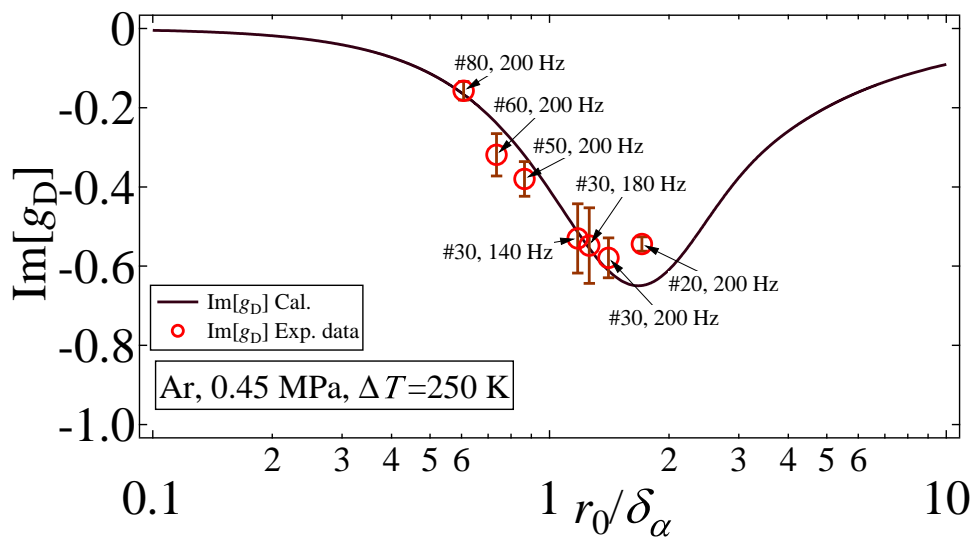
Figure 5. Relation between Im $[g_D]$ and r_0/δ_α. The curve of Im $[g_D]$ was calculated from the thermoacoustic theory. The symbols represent the experimental values evaluated from Equation (14) with measured data and the thermal properties of the gas at the hot end of the regenerator ($T_H = 543$ K).

Thermoacoustic theory describes that the flow resistance of the regular flow channel is a constant [17–19], independent of the velocity amplitude, whereas that in the porous media with tortuous flow channels is shown to increase with the velocity [28–30] or Reynolds number [2–5,7]. From measurements of the acoustic field, we have proposed modification of the effective radius r_0 to have velocity dependence [16] as

$$r_{\text{eff}} = 2\delta_\nu \left(\frac{0.8\nu}{\omega d_h^2} Re_h + \frac{16\delta_\nu^2}{d_h d_w} \right)^{-\frac{1}{2}}.$$

(15)

The effective radius r_{eff} approaches r_0 when the velocity is negligibly small. It decreases concomitantly with increasing velocity. Figure 6 presents a comparison of the effective radii in Equation (15) and that obtained with the experimental acoustic fields of #30 and #80 mesh screens given in Figure 4. We have determined the experimental effective radius shown by symbols in the way that the difference of the calculated acoustic powers from the measured acoustic powers at two ends of the regenerator [16] is minimized. Because the experimental effective radius reflects all mesh screens stacked in the regenerator holder, the kinematic viscosity ν in Equation (15) is evaluated at average temperature $(T_R + T_H)/2$. In addition, the horizontal axis represents the spatial average velocity amplitude $|V_m|$ over the regenerator area. The experimental effective radii were obtained with error $< 8\%$ between the measured and calculated acoustic powers. It apparently decreases with velocity $|V_m|$. Therefore, the acoustic field at the sides of the regenerator is better estimated using effective radius r_{eff} than r_0, when the velocity amplitude is finite.

Figure 7 presents comparison of the heat flow rates $|Q|$ obtained by inserting r_0 and r_{eff} into Equations (3) and (4). Results show that $|Q|$ obtained with r_{eff} yields a faulty result because it goes away from that obtained with r_0 with increasing $|\langle V \rangle|$. This result indicates that r_0 should be used instead of r_{eff} for better estimation of heat flow. Other earlier studies [29,31] have demonstrated that two effective radii are necessary to explain the viscous behavior and the thermal behavior in tortuous porous media because the viscous effects are governed by narrower regions of the channel, whereas the thermal effects are determined by wider regions [32,33]. Our experimentally obtained results provide another example representing the need of the effective thermal radius, in addition to the effective viscous radius.
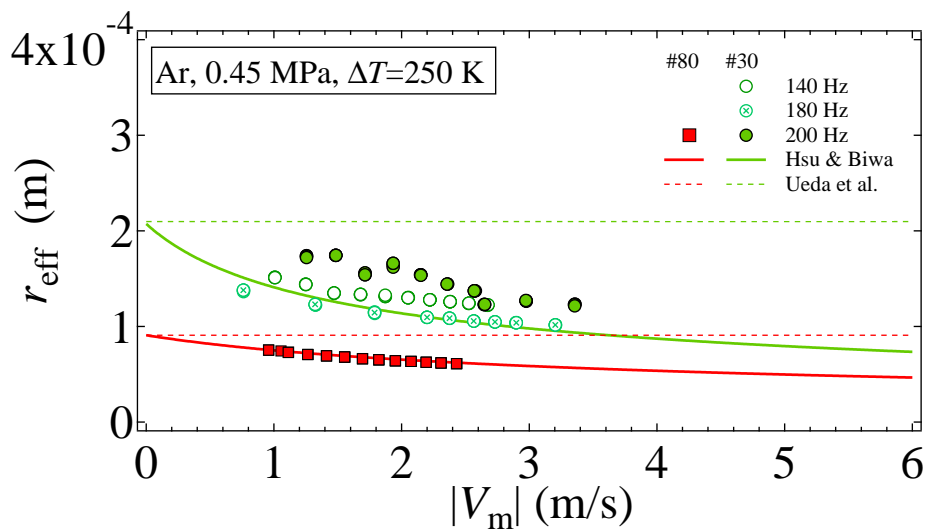
Figure 6. Relation between r_{eff} and $|V_m|$. Symbols represent the experimental effective radius of the stacked-screen regenerator of #30 and #80 meshs. Curves stand for Equation (15) with thermal properties of the gas determined from a temperature averaged in T_R and T_H. Horizontal dashed lines represents the effective radius r_0 of Ueda et al.
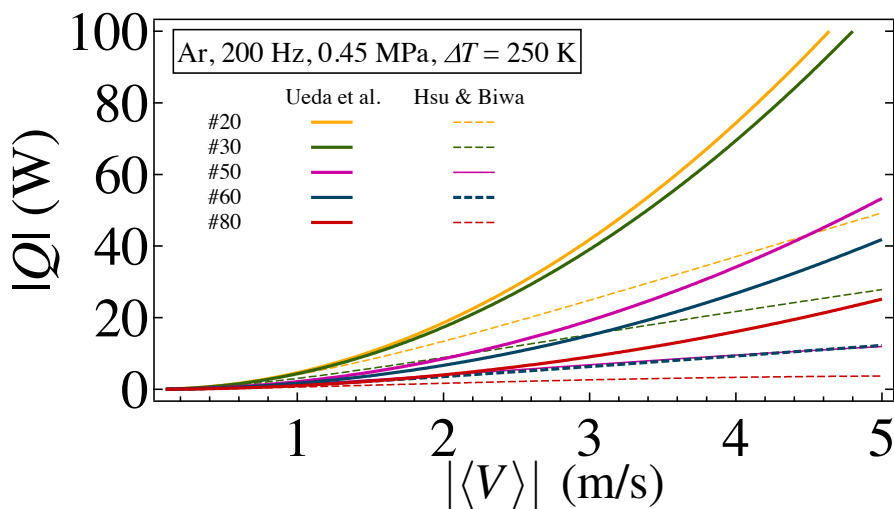

Figure 7. Comparisons between predictions of heat flow $|Q|$ given, respectively, by the effective radius of Ueda et al. and Hsu and Biwa, for stacked-screen regenerators in pressurized argon gas with 0.45 MPa and oscillation frequency of 200 Hz.

5. Conclusions

Heat transport through the stacked screen regenerators has been investigated experimentally in Ar gas with mean pressure of 0.45 MPa. The measured heat flow rates are compared with those calculated from four empirical equations, parameterized by r_0/δ_α and/or Re_h. Results have shown that all the empirical equations tested reproduce the measured heat flow rates to a mutually similar extent. Among those empirical equations, Ueda's formulation based on the effective radius r_0 involves the simplest derivation of the heat flow rate. Therefore, it is expected to be useful for designing thermoacoustic Stirling engines. However, the acoustic field, especially the acoustic power, can be described better by the effective radius r_{eff}, which decreases with the velocity amplitude. Therefore, it is necessary to use two effective radii to account for the viscous behavior and the thermal behavior of the gas in the stacked screen regenerators.

Author Contributions: Tetsushi Biwa conceived the research plan. Shu Han Hsu designed and performed the experiments and prepared the manuscript. Tetsushi Biwa revised the manuscript. Both authors have read and approved the final manuscript.

Conflicts of Interest: The authors declare no conflict of interest.

References

1. Backhaus, S.; Swift, G.W. A thermoacoustic Stirling heat engine. *Nature* **1999**, *399*, 335–338.
2. Tong, L.S.; London, A.L. Heat-transfer and flow-friction characteristics of woven-screen and cross-rod matrices. *Trans. ASME* **1957**, *10*, 1558–1570.
3. Tanaka, M.; Yamashita, I.; Chisaka, F. Flow and heat transfer characteristics of the Stirling engine regenerator in an oscillating flow. *JSME Int. J.* **1990**, *33*, 283–289.
4. Gedeon, D.; Wood, J.G. *Oscillating-Flow Regenerator Test Rig: Hardware and Theory With Derived Correlations for Screens and Felts*; NASA Contractor Report 198442; NASA-Lewis Research Center: Cleveland, OH, USA, 1996.
5. Isshiki, S.; Sakano, A.; Ushiyama, I.; Isshiki, N. Studies on flow resistance and heat transfer of regenerator wire meshes of Stirling engine in oscillatory flow. *JSME Int. J. Ser. B* **1997**, *40*, 281–289.
6. Zhao, T.S.; Cheng, P. Oscillatory heat transfer in a pipe subjected to a laminar reciprocating Flow. *Int. J. Heat Mass Transf.* **2005**, *48*, 2473–2482.
7. Costa, S.C.; Tutar, M.; Barreno, I.; Esnaola, J.A.; Barrutia, H.; García, D.; González, M.A.; Prieto, J.I. Experimental and numerical flow investigation of Stirling engine regenerator. *Energy* **2014**, *72*, 800–812.
8. Wheatley, J.; Hofler, T.; Swift, G.W.; Migliori, A. An intrinsically irreversible thermoacoustic heat engine. *J. Acoust. Soc. Am.* **1983**, *74*, 153–170.
9. Tijani, M.E.H.; Spoelstra, S. A high performance thermoacoustic engine. *J. Appl. Phys.* **2011**, *110*, 093519.
10. Wu, Z.; Man, M.; Luo, E.; Dai, W.; Zhou, Y. Experimental investigation of a 500 W traveling-wave thermoacoustic electricity generator. *Chin. Sci. Bull.* **2011**, *56*, 1975–1977.
11. Yu, Z.; Jaworski, A.J.; Backhaus, S. Travelling-wave thermoacoustic electricity generator using an ultra-compliant alternator for utilization of low-grade thermal energy. *Appl. Energy* **2012**, *99*, 135–145.
12. Smoker, J.; Nouh, M.; Aldraihem, O.; Baz, A. Energy harvesting from a standing wave thermoacoustic-piezoelectric resonator. *J. Appl. Phys.* **2012**, *111*, 104901.
13. Wang, K.; Sun, D.; Zhang, J.; Xu, Y.; Luo, K.; Zhang, N.; Zou, J.; Qiu, L. An acoustically matched traveling-wave thermoacoustic generator achieving 750 W electric power. *Energy* **2016**, *103*, 313–321.
14. Flitcroft, M.; Symko, O.G. Ultrasonic thermoacoustic energy converter. *Ultrasonics* **2013**, *53*, 672–676.
15. Obayashi, A.; Hsu, S.H.; Biwa, T. Amplitude dependence of thermoacoustic properties of stacked wire meshes. *J. Cryog. Soc. Jpn.* **2012**, *47*, 562–567. (In Japanese)
16. Hsu, S.H.; Biwa, T. Modeling of a stacked-screen regenerator in an oscillatory flow. *Jpn. J. Appl. Phys.* **2016**, *56*, 017301.
17. Swift, G.W. Thermoacoustics: A Unifying Perspective for Some Engines and Refrigerators. *J. Acoust. Soc. Am.* **2002**, doi:10.1121/1.1561492.
18. Tominaga, A. *Fundamental Thermoacoustics*; Uchida Rokakuho Publishing Co.: Tokyo, Japan, 1998; Chapter 7. (In Japanese)
19. Tominaga, A. Thermodynamic aspects of thermoacoustic theory. *Cryogenics* **1995**, *35*, 427–440.
20. Ueda, Y.; Kato, T.; Kato, C. Experimental evaluation of the acoustic properties of stacked-screen regenerators. *J. Acoust. Soc. Am.* **2009**, *125*, 780–786.
21. Hasegawa, S.; Ashigaki, Y.; Senga, M. Thermal diffusion effect of a regenerator with complex flow channels. *Appl. Therm. Eng.* **2016**, *104*, 237–242.
22. Swift, G.W.; Ward, W.C. Simple harmonic analysis of regenerators. *J. Therm. Heat Transf.* **1996**, *10*, 652–662.
23. Kays, W.M.; London, A.L. *Compact Heat Exchangers*; McGraw-Hill: New York, NY, USA, 1964.
24. Ward, B.; Clark, J.; Swift, G.W. *Design Environment for Low-Amplitude ThermoAcoustic Energy Conversion (DeltaEC) User's Guide (Version 6.3)*; Los Alamos National Laboratory: Los Alamos, NM, USA, 2012.
25. Gedeon, D. *Sage User's Guide (v11 Edition)*; Gedeon Associates: Athens, OH, USA, 2016.

26. Fusco, A.; Ward, W.; Swift, G.W. Two-sensor power measurements in lossy ducts. *J. Acoust. Soc. Am.* **1992**, *91*, 2229–2235.

27. Biwa, T.; Tashiro, Y.; Nomura, H.; Ueda, Y.; Yazaki, T. Experimental verification of a two-sensor acoustic intensity measurement in lossy ducts. *J. Acoust. Soc. Am.* **2008**, *124*, 1584–1590.

28. Wilson, D.K.; McIntosh, J.D.; Lamber, R.F. Forchhemer-type nonlinearities for high-intensity propagation of pure tones in air-saturated porous media. *J. Acoust. Soc. Am.* **1988**, *84*, 350–359.

29. McIntosh, J.D.; Zuroski, M.T.; Lambert, R.F. Standing wave apparatus for measuring fundamental properties of acoustic materials in air. *J. Acoust. Soc. Am.* **1990**, *88*, 1929–1938.

30. McIntosh, J.D.; Zuroski, M.T. Nonlinear wave propagation through rigid porous materials. I: Nonlinear parameterization and numerical solutions. *J. Acoust. Soc. Am.* **1990**, *88*, 1939–1949.

31. Roh, H.; Raspet, R.; Bass, H.E. Parallel capillary-tube-based extension of thermoacoustic theory for random porous media. *J. Acoust. Soc. Am.* **2007**, *121*, 1413–1422.

32. Zwikker, C.; Kosten, C.W. *Sound Absorbing Materials*; Elsevier: Amsterdam, The Netherlands, 1949; Chapter 2.

33. Petculescu, A.; Wilen, L.A. Lumped-element technique for the measurement of complex density. *J. Acoust. Soc. Am.* **2001**, *110*, 1950–1957.